PAPER Nr. : 10

EXPERIMENTAL INVESTIGATION OF THE SWEEP EFECTS ON A HELICOPTER BLADE TIP

by

Mrs. R. Imbert and Mr. J.J. Thibert
ONERA, 92320 Châtillon, FRANCE

TENTH EUROPEAN ROTORCRAFT FORUM

AUGUST 28 – 31, 1984 – THE HAGUE, THE NETHERLANDS

Abstract

An experimental study was made on a half-wing in steady transonic flow. The model represented a helicopter blade tip with a rectangular planform. Tests were at three sweep angles, φ = 0°, + 30° and - 30°, with Mach numbers and angles of attack corresponding to various helicopter flight modes. The tests showed that the 3-D effects were small at zero sweep, with the same pressure distributions as measured in 2-D flow on the various wing profiles. The positive and negative sweep tests brought out the strong asymmetry of the flow in transonic regime at identical sweep values, the extension of the supersonic zones for the two sweep values, and increased overspeeds and shock intensity on the outboard part of the wing in positive sweep position. The computation methods have been validated by comparison with experiment. They calculate the transonic 3-D flow by solving either the full potential equation or the small disturbances equation. Some calculations including the viscosity showed its secondary effects for the advancing blade but its large effects for the retreating blade.

Notations

M_0 Mach number at infinity

φ sweep angle

C_L coefficient of lift

C_D coefficient of drag

K_p pressure coefficient

Mdx drag divergence Mach number

α angle of attack

x distance along chord

y spanwise distance

z distance perpendicular to the (x, y) plane

1. Introduction

The improvement that new blade tip designs have brought in helicopter performance has stimulated a great deal of research throughout the world, and in particular at ONERA. To define these new shapes requires an intimate knowledge of the flow itself, along with computation methods for predicting this flow, and thus the blade performance, correctly.

The flow near a blade tip depends both on the unsteady effects and on the 3-D effects due to the variation in the sweep angle (Fig. 1). Direct measurements on a rotor [1] have shown that sharp asymmetries exist in the flow at the same azimuth angle, with the blade advancing and retreating. These are due partly to the 3-D effects, which cannot be distinguished from the unsteady effects in the actual rotor measurements.

This is why a blade tip analysis was undertaken in steady flow, specially oriented toward studying the 3-D effects. Measurements were made on a half-wing model representing a helicopter blade tip for sweep angles of 0°, + 30° and - 30°. These measurements also served to validate the transonic steady flow computations used at ONERA. Below, we will first present the model and the main experimental data at zero sweep. The sweep effects for the various Mach and lift conditions corresponding to the advancing and retreating blade, and to hovering flight, will then be discussed. The final section compares the experimental data with the calculation methods.

2. The experimental study

2.1. The model

The wing is rectangular, with an aspect ratio of 3, simulating a helicopter blade tip. The inboard half of the wing is an OA 209 profile. The outboard half tapers down to the OA 207 tip section (Fig. 2). The wing is wall-mounted in the Chalais-Meudon S3 wind tunnel. This return circuit tunnel has a nearly octagonal test section, inscribed in a one-meter diameter (Fig. 3). The top and bottom walls are perforated and the Mach number ranges from 0.3 to 1. The model is mounted on the side wall at a controllable sweep angle (Fig. 4), with 392 pressure taps fitted in eight sections along the span of the wing.

2.2. Tests

The measurements made were :

- stress measurements with a wall balance, for the zero sweep tests,

- pressure measurements for the three sweep angles.

The test conditions included the main helicopter operating modes, i.e. forward flight, hovering and maneuvering. The Reynolds number with respect to the chord of the model (148 mm) varied from 1.04×10^6 (at $M_0 = 0.3$) to 1.4×10^6 (at $M_0 = 0.8$). The tests were carried out in natural transition.

2.3. Zero sweep data

The overall stresses were measured at zero sweep. The lift variations are shown in figure 6 as a function of the angle of attack, for Mach numbers going from 0.4 to 0.85. Stall occurs around 12° at $M_0 = 0.4$, and the C_{Lmax} is 1.02. The C_{L_α} slopes increase up to $M_0 = 0.8$, beyond which nonlinearities appear at low angles of attack.

The drag forces calculated from model weighings were used to define a constant C_L drag divergence Mach number, assuming $dC_X/dM = 0.1$.

The wing C_{Lmax} for Mach numbers below 0.4 is shown in figure 7 along with the constant C_L drag divergence Mach numbers for Mach numbers over 0.78 and the corresponding performance of the OA 209 and OA 207 airfoils in 2-D tests. The wing C_{Lmax} is of course less than that of the airfoils, due to the aspect ratio effects, and the drag divergence Mach number is between the values obtained for the airfoils.

When the blade is advancing, at $C_L = 0$, the wing Mdx is 0.865. The corresponding iso-Mach lines are shown in figure 8. The iso-Mach lines on the upper surface (Fig. 8 a) show the shock at 50 % chord, midspan, approaching the leading edge in the outboard sections. This matches the 2-D data on the OA 209 and OA 207 airfoils shown in Fig. 8 b. The spanwise overspeed maxima are approximately constant and the 3-D effects are moderate. The 2-D distributions are also confirmed on the lower surface (Fig. 8 c). Thus the post-shock re-acceleration on OA 209 are also present on the inboard sections of the wing, while the recompression is continue on the outboard part, as on the OA 207.

At $M_0 = 0.6$ and $C_L = 0.6$ (hovering) (Fig. 9 a), the upper surface flow is two-dimensional out to midspan. The overspeeds increase near the leading edge on the outboard section because of the induced angle of attack. The supersonic zone is, as on the individual profiles (Fig. 9 b) limited to some 10 % of the chord.

Under the retreating blade conditions ($M_0 = 0.4$), the C_L (α) curve (Fig. 10) shows the classical aspect ratio effects with a reduction in the slope and in C_{Lmax}, with respect to the OA 207 and OA 209 profiles. The stall angle is intermediate between those of the airfoils. The upper surface iso-Mach lines (Fig. 11) for 11°, 12° and 13° show that the separation first appears on the inboard side of the wing and gradually propagates to the tip, where the vortex modifies the velocity field. The stall is of the trailing edge type with the overspeeds near the leading edge continuing to increase with angle of attack.

The zero sweep test data thus show that the aerodynamic behavior of the wing for the three main blade tip operating modes is close to that of the airfoils in 2-D flow, except for the aspect ratio effects at high C_L.

2.4. Effect of the sweep

The test conditions at $\pm$ 30° sweep were such as to duplicate the zero sweep test conditions for the Mach number and angle of attack normally referenced to the leading edge.

For a normal Mach number of 0.805 and a normal angle of attack - 1.5°, figure 12 shows the strong asymmetry of the upper surface iso-Mach lines for the two sweep angles. At positive sweep (Fig. 12 a), the supersonic zone is much more extensive than at zero sweep (Fig. 12 b). The overspeeds are higher over the outboard section where the closeness of the iso-Mach lines shows that the shock is more intense while the recompression is more gradual at midspan. At negative sweep (Fig. 12 c), on the other hand, the overspeeds are higher on the inboard part of the wing. The supersonic zones extends over the greater part of the wing and no shock appears, as the recompressions are much weaker than at zero sweep. The disturbances created by the tip vortex can also be observed at negative sweep. The same tendencies are found on the lower surface (Fig. 13), i.e. extension of the supersonic zone for the two sweep angles, compared to the zone at zero sweep, increased overspeeds and recompression gradients at the tip for the positive sweep, increaded overspeeds on the inboard side and no shock for the negative sweep.

As the normal Mach number increases, the asymmetry becomes more pronounced, with an upper surface shock located much farther downstream than at zero sweep for a normal Mach number of 0.831. The supersonic zone is very extensive at negative sweep, with much higher overspeeds on the inboard side than at zero sweep ; but the recompressions are gradual and the iso-Mach lines show no shock wave. The lower surface iso-Mach lines show the same phenomena under the same conditions (Fig. 15).

Under hovering flight conditions (M_0 = 0.6, Fig: 16), since the supersonic zone does not extend very far over the upper surface at zero sweep, the asymmetries are less pronounced than before and the flow is more two-dimensional. Nonetheless, the displacement of the maximum overspeeds, and the increase of the recompression gradients from the inboard part of the wing outward should be noted, when the sweep angle goes from - 30° to + 30°.

At low Mach number (M_0 = 0.4), the flow is slightly supersonic in the immediate vicinity of the upper surface leading edge, at 11° angle of attack. Under these conditions, the sweep has little effect on the flow over the wing (Fig. 17). It will nonetheless be noted that the tendency to separate on the inboard side is suppressed at positive sweep and becomes more pronounced at negative sweep, with an increase in the recompression gradients near the leading edge. The iso-Mach lines at negative sweep also show the disturbances the tip vortex creates in the vicinity of the tip.

The highly three-dimensional aspects of the flow and the nonlinearity of the sweep effect were thus clearly brought out by these tests. Yet it should be emphasized that the relatively small aspect ratio of the model results in a non-negligible effect of the wind tunnel wall on the flow structure on the inboard part of the wing, especially at negative sweep angles in transonic flow. This increases the overspeeds in this region, which would not be the case on a blade tip with a much higher aspect ratio. However, on the outer part of the wing, which simulates the blade tip, the side wall effects are weak and the simulation is realistic in these tests.

3. Comparison with calculations

This test data was used to validate the methods for calculating the 3-D flow around wings developed at ONERA. There are two types of methods. The first solves the full potential equation and is used for fixed wings [2]. This has just been adapted to the calculation of quasi-steady flows around helicopter blades. The second type of method solves the equation of small unsteady disturbances. This is the method commonly used for helicopter blade calculations at ONERA [3].

3.1. - Description of the Computation Methods

- Full Potential Equation:(FPE) Method.

With this method, the full potential equation is solved in nonconservative form, expressed as a system of curvilinear coordinates (ξ , η , ζ):

$$\mathcal{L}\phi = A\phi_{\xi\xi} + B\phi_{\eta\eta} + C\phi_{\zeta\zeta} + D\phi_{\xi\eta} + E\phi_{\xi\zeta} + F\phi_{\eta\zeta} + G = 0.$$

The coordinates (ξ , η , ζ) are those of the rectangular grid of the calculation plane, and the coefficients A, B, C, D, E, F and G depend on the components of the velocity and of the metric tensor of the conversion going from the (ξ , η , ζ) calculation plane to the physical (x, y, z) plane.

The algorithm uses a finite difference technique from Chattot [4]. The second derivatives are approximated by centered differences in subsonic flow. When the flow is locally supersonic, a combined centered/off-centered difference scheme is used. The equations are solved by a relaxation-by-column technique. The grid is found by a parabolic conversion giving C-shaped grids in each plane parallel to the plane of symmetry. The grids for the calculations have 210 x 29 x 30 points.

- Small Disturbance Equation:(SDE) Method.

This method solves the small transonic disturbances equation :

$$A\phi_{tt} + B\phi_{xt} = F_x + \phi_{33} + C\phi_{yy} + D\phi_{xy} .$$

F is a nonlinear term that is a function of ϕ_x and ϕ_t. This method, detailed in [5], is solved for the applications presented in this paper in its quasi-steady form, in which the time derivatives are ignored. The calculation space in the same as the one used in the FPE method. The equation, expressed in the calculation space coordinate system, is discretized in conservative form and solved by an ADI method. The Cartesian grids have 70 x 17 x 30 points.

For the calculations carried out at $\pm$ 30° sweep, the planform of the wing was modified to align the free end of the wing with the direction of flow upstream. This was done in such a way as to maintain the real aspect ratio of the wing (Fig. 18).

3.2. Results

3.2.1. - Zero sweep

The upper surface iso-Mach lines calculated by both methods are compared with the experimental data in figure 19 for a Mach number of 0.831 and a - 1.5° angle of attack. The results obtained with the two methods are very close. We will only note that the shock calculated by the SDE method is slightly farther downstream, because of the conservative scheme. Compared to experiment, the results are very good. The calculations correctly reconstruct the position of the shock in the various sections, and the downstream recompression. Nonetheless, the calculations slightly overestimate the maximum overspeed in the supersonic region at the wing tip.

The lower surface calculations (Fig. 20) are also very close to each other, the only difference residing in the acceleration following the shock, which the FPE method predicts to be more extensive in the spanwise direction than the SDE method. This difference can be attributed to the different schemes--the conservative scheme in the SDE method giving a lower speed level after the shock than the conservative scheme in the FPE method. The same re-acceleration results in higher Mach levels for the FPE method. This overspeed zone is less extensive in experiment than in the calculations, because of the viscosity. At Mach 0.6, C_L = 0.6 (Fig. 21), the extent of the supersonic zone near the leading edge is slightly underestimated by the SDE method and very well predicted by the FPE method. On the other hand, the iso-Mach lines calculated in the recompression region are very close to the experimental data, for both methods.

At Mach 0.4 and 11° of angle of attack (Fig. 22), the SPE method underestimates the leading edge overspeeds, which are overestimated in the FPE method. These tendencies are consistent with the hypothesis of the small disturbances used in the SDE method, and with the absence of viscous effects in the FPE method. This absence of viscous effects also results in the fact that neither of the two methods predicts the experimentally observed separation tendency in the inboard sections of the airfoil.

3.2.2. Sweep effect

At + 30° sweep for a normal Mach number of 0.835 and a normal angle of attack - 1.5°, figure 23 shows that the two methods provide a qualitative reconstruction of the main flow characteristics, i.e. the existence of higher overspeeds toward the tip and a more extensive supersonic zone that at zero sweep. We nonetheless observe that, in the SDE method, the shock is not very clear in the outboard region because of the relatively low density of the mesh. For the FPE method, the shock appears clearly and its midspan abscissa is quite accurate. The experimental data places the shock farther downstream than the calculations do, on the outboard part of the wing, and the overspeeds are not as high. These differences are probably due to the fact the free edge of the wing in the experiment was not aligned with the direction of the upstream flow, as was the wing in the calculations. This increases the load at the tip.

The comparison of computed and experimental data for the lower surface (Fig. 24) is not quite as good. The FPE method errors in the position of the shock are larger than for the upper surface, and the SDE method predicts the shock and overspeeds poorly on the outboard part.

At negative sweep, both on the upper surface (Fig. 25) and lower surface (Fig. 26), the FPE method correctly predicts the extent of the supersonic and the levels of the overspeeds. As the Mach gradients are small, the iso-Mach lines resulting from interpolations have different shapes. We will also observe the size of the overspeeds and the high shock intensity near the side wall, in the sections not fitted with pressure holes.

For a normal Mach number of 0.6 and $C_L = 0.6$, both at positive (Fig. 27) and negative (Fig. 28) sweep, the calculations with the FPE method predict very well the flow over the wing with iso-Mach lines close to those calculated from the test data, except in the vicinity of the tip at negative sweep.

3.3. Viscous Effects

A few calculations were carried out to evaluate viscous effects. The calculation method used was from Lazareff and Le Balleur [6], which couples the FPE method described above with a 3-D laminar turbulent method for calculating the boundary layers. The wake is not included in this method and the transition is determined by the Granville criterion (longitudinal instability) or by the Baisley (transverse instability) or Russel criterion (laminar separation bubble). The boundary layer calculation gives the transpiration velocity field, which is used as a boundary condition in the inviscid flow calculation. The process is iterative, with under-relaxation of the viscous effects, to converge the coupling.

In the present case, where the wing consists of thin profiles with no rear load, the viscous effects are moderate at low lift. This is shown in figure 29, which gives the pressure distributions calculated for different spanwise sections when $M_0 = 0.831$, $\varphi = 0$ and $C_L \simeq 0$ in inviscid and in viscous flow. We can observe the very slight advance of the upper and lower shocks and the decreased re-acceleration following the lower surface shock, which agrees with the experimental data.

For a 30° sweep and the same Mach and angle of attack conditions referenced normal to the leading edge, with the shock farther downstream than at zero sweep, the effect of the viscosity is greater, in particular on the inboard sections of the wing (Fig. 30).

If the viscosity has little effect under advancing blade conditions, the same is not true under retreating blade conditions where taking the viscous effects into account greatly reduces the leading edge overspeed and the general level of the lift (Fig. 31).

4. Conclusions

The following conclusions can be drawn from the experimental study, in steady flow, on a half-wing simulating a helicopter blade tip :

- At zero sweep, the measured pressure distributions for different helicopter flight configurations are very close to the pressure distributions measured in 2-D flow on the separate profile sections making up the wing.

- The sweep effects are large in transonic flow and are highly nonlinear. The positive sweep creates high overspeeds and intense shocks in the vicinity of the tip. On the other hand, the negative sweep increases the overspeeds on the inboard part ; but although supersonic zone is more extensive than at zero sweep, the recompression gradients are smaller and the recompressions are isentropic.

The comparison of calculated and experimental data for the various Mach and sweep conditions show that :

- the computation method based on solving the full potential equation makes it possible to predict the wing tip flow correctly even under the most difficult conditions (high Mach and sweep).

- the computation method solving the small disturbances equation also gives excellent results at zero sweep and predicts the sweep effects qualitatively ; but errors appear in the position and intensity of the shock, at least for high Mach and sweep values.

- the viscous effects are moderate under advancing blade conditions, even when the sweep angle is large. They are, however, very high in the retreating blade configuration.

New planforms, in particular for high helicopter tip speed ratios, should be defined using methods that correctly predict the 3-D and unsteady effects, as the non-inclusion of these effects could produce design that are thoroughly inadapted to the real operating conditions of the blade.

The authors wish to thank Messrs. Chaumet, Desopper and Destarac for their help in writing this paper.

References

[1] J.J. Thibert and J.J. Philippe, Studies of airfoils and blade tips for helicopters, La Recherche Aérospatiale, 1982-4

[2] B. Chaumet, D. Destarac, T.H. Lê, Three dimensional computational methods applied to aerodynamic analysis of transonic flows past a wing body configuration, 14th ICAS meeting, 1984, Toulouse, France

[3] J.J. Philippe et A. Vuillet, Conception aérodynamique de futurs rotors avec de nouvelles formes d'extrémité de pale, 39e Forum "AHS", St Louis Missouri, 9-11 mai 1983, ONERA TP 1983-119

[4] J.J. Chattot, C. Coulombeix et C. Da Silva Tomé, Calculs d'écoulements transsoniques autour d'ailes, La Recherche Aérospatiale, n° 4, pp. 143-158, 1978

[5] J.J. Chattot and J.J. Philippe, Pressure distribution computation on a non lifting symmetrical helicopter blade in forward flight, La Recherche Aérospatiale n° 1980-5

[6] J.C. Le Balleur, M. Lazareff
Computation of three-dimensional viscous flows on transonic wings via boundary layer-inviscid flow interaction, La Recherche Aérospatiale, n° 1983-3

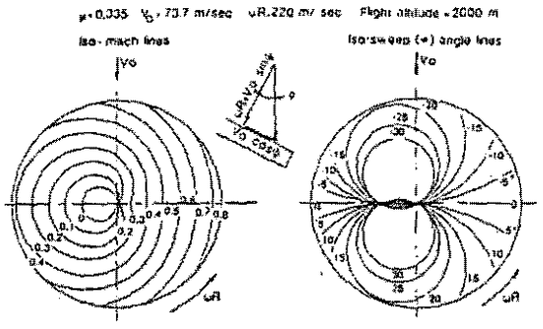

Fig. 1 – Iso-Mach lines and iso-sweep-angle lines.

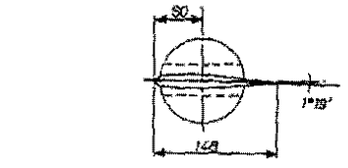

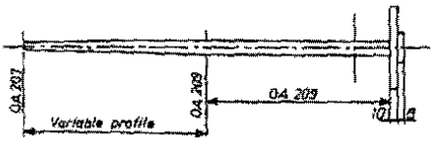

Fig. 2 – Experimental model.

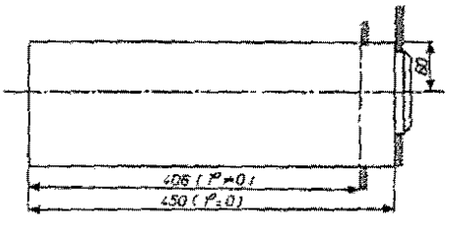

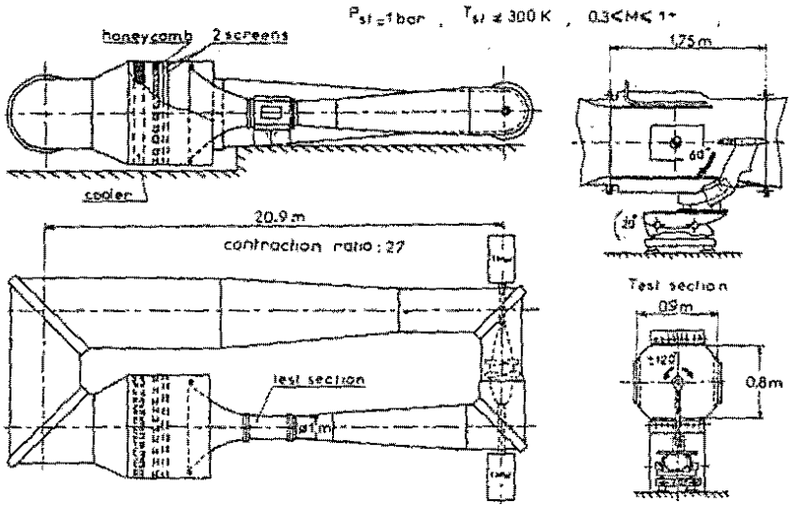

Fig. 3 – S3 Chalais-Meudon wind tunnel.

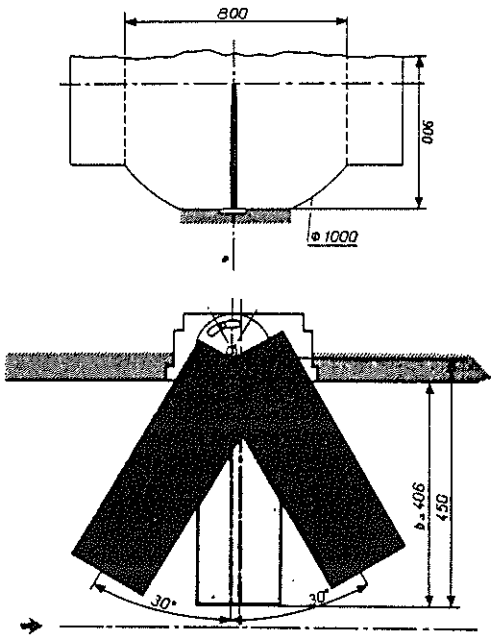

Fig. 4 — Sweep variation.

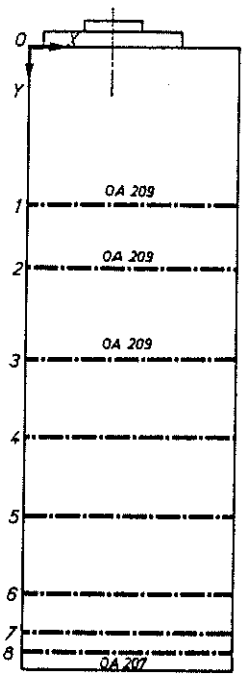

Fig. 5 — Sections with pressure measurements.

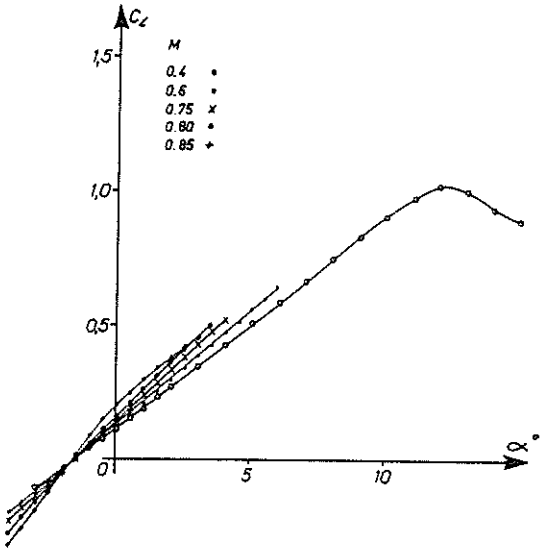

Fig. 6 — Lift at zero sweep.

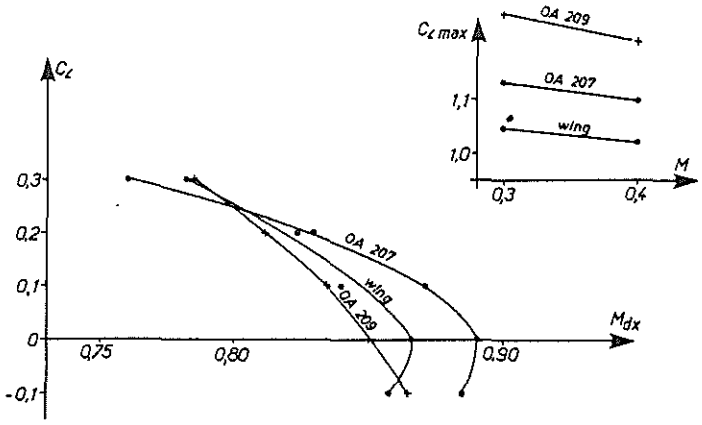

Fig. 7 — Total performance at zero sweep.

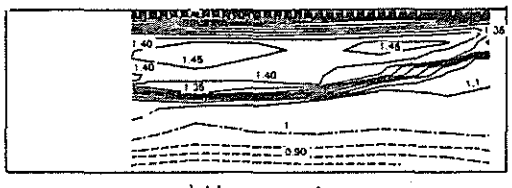

a) Upper surface

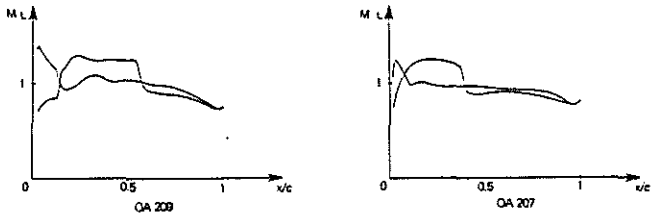

b) OA 209 and OA 207 profiles

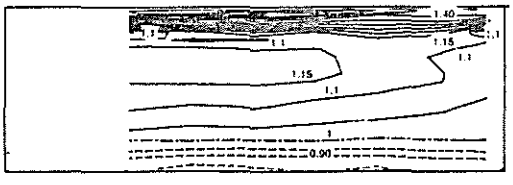

c) Lower surface

Fig. 8 — Iso-Mach lines. Forward flight $M_0 = 0.86$, $C_L = 0$, $\alpha = -1.^\circ 5$ (zero sweep).

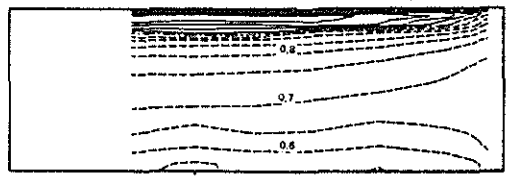

a) Upper surface

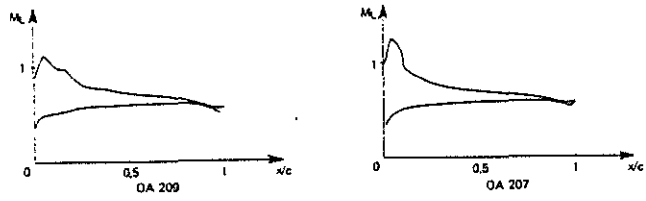

b) OA 209 and OA 207 profiles

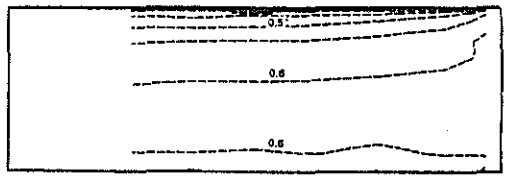

c) Lower surface

Fig. 9 — Iso-Mach lines. Hovering flight $M_0 = 0.6$, $C_L = 0.6$, $\alpha = 5.^\circ 6$ (zero sweep).

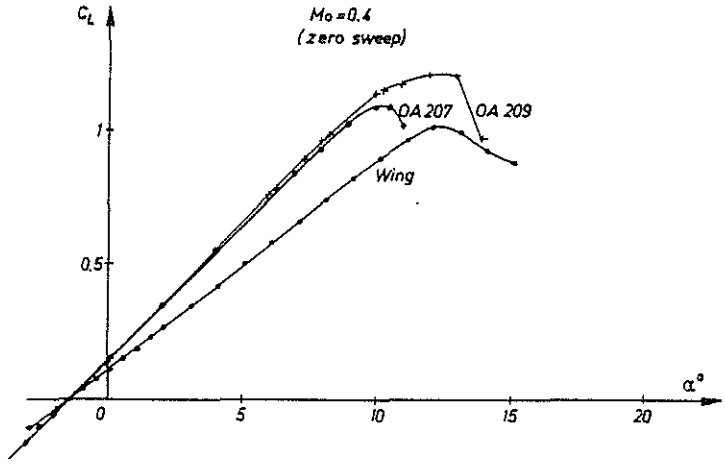

Fig. 10 — Lift under the retreating blade conditions.

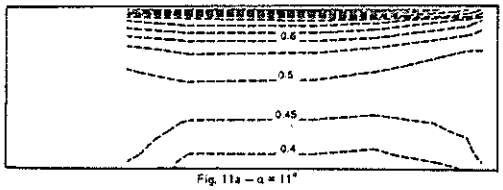

Fig. 11a – α = 11°

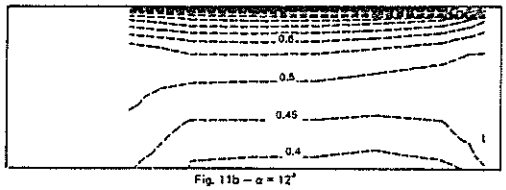

Fig. 11b – α = 12°

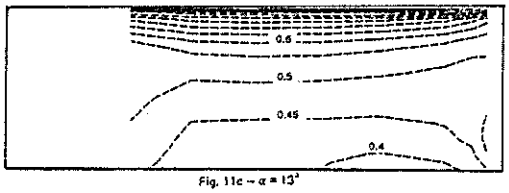

Fig. 11c – α = 13°

Fig. 11 — Iso-Mach lines on the upper surface near the stall. Retreating blade conditions $M_0 = 0.4$ (zero sweep).

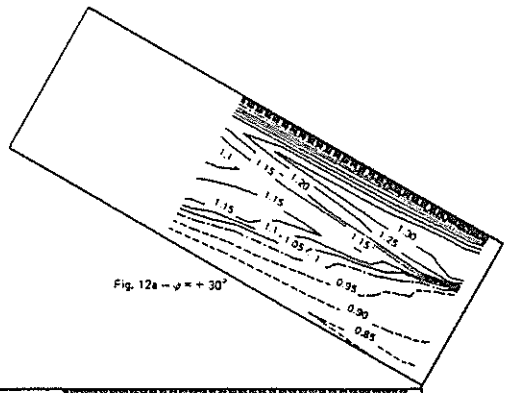

Fig. 12a – ψ = + 30°

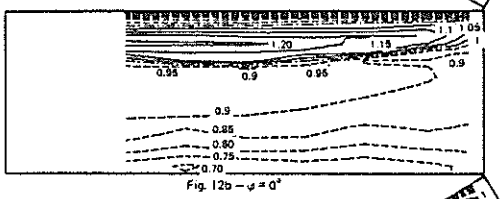

Fig. 12b – ψ = 0°

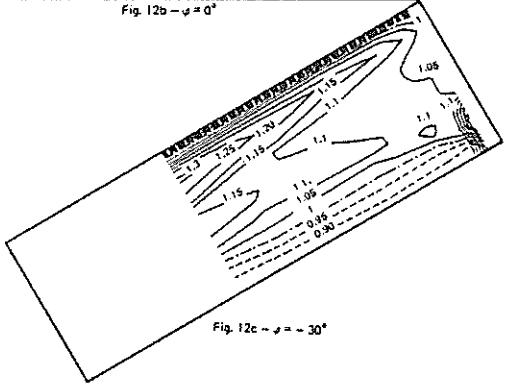

Fig. 12c – ψ = – 30°

Fig. 12 — Iso-Mach lines on the upper surface . $M_N = 0.805$; $\alpha_N = -1.5°$.

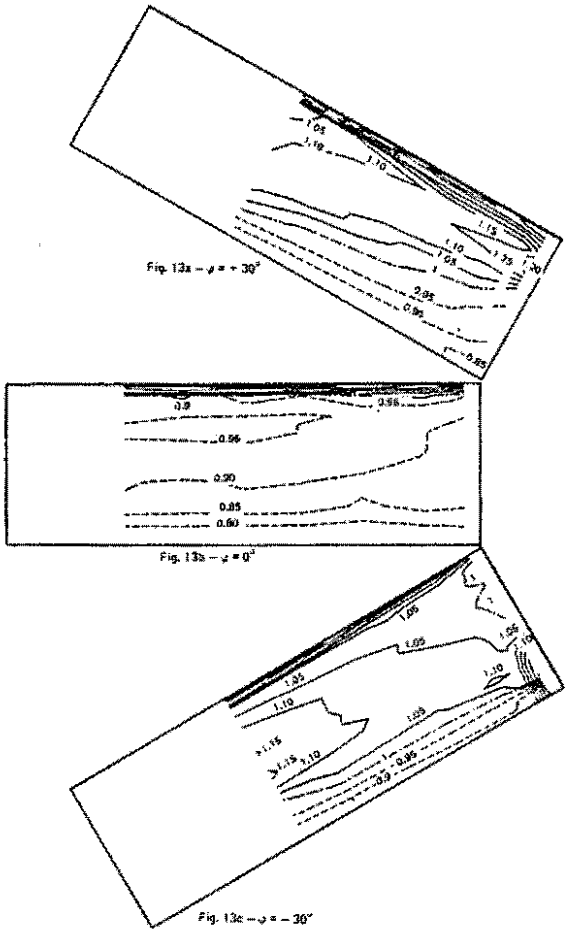

Fig. 13 — Iso-Mach lines on the lower surface . $M_N = 0.805$; $\alpha_{\overline{N}} - 1.^{\circ}5$.

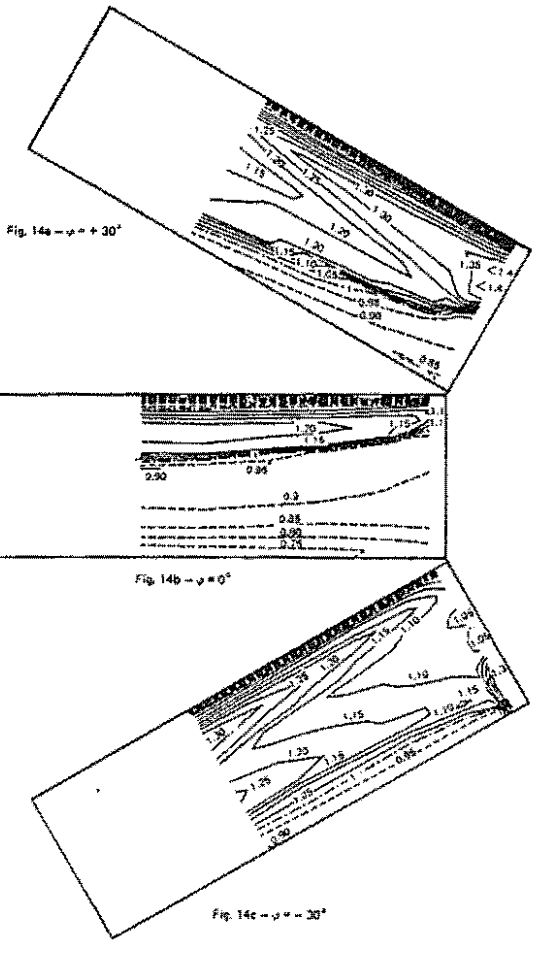

Fig. 14 — Iso-Mach lines on the upper surface . $M_N = 0.831$; $\alpha_{\overline{N}} - 1.^{\circ}5$.

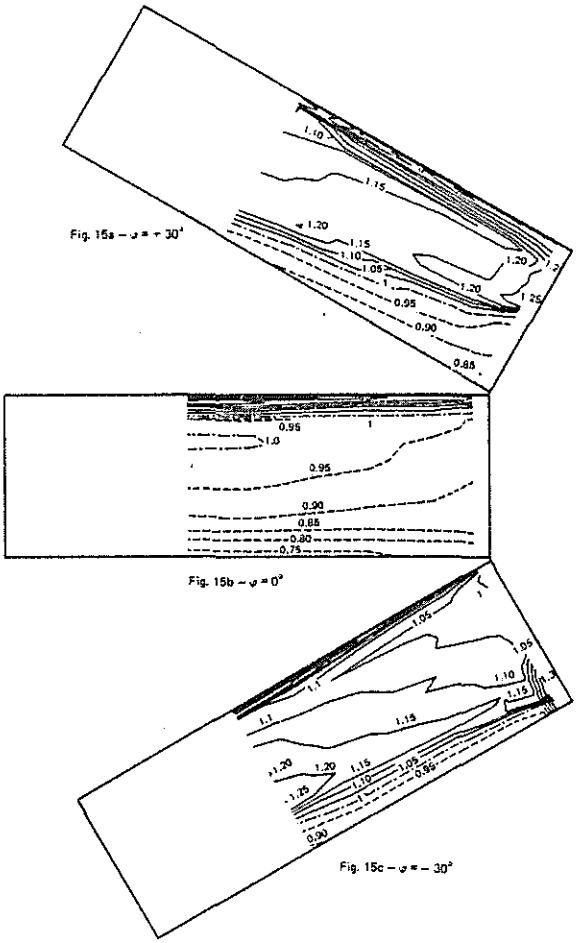

Fig. 15 – Iso-Mach lines on the lower surface . $M_N = 0.831$; $\alpha_N = -1.^\circ 5$.

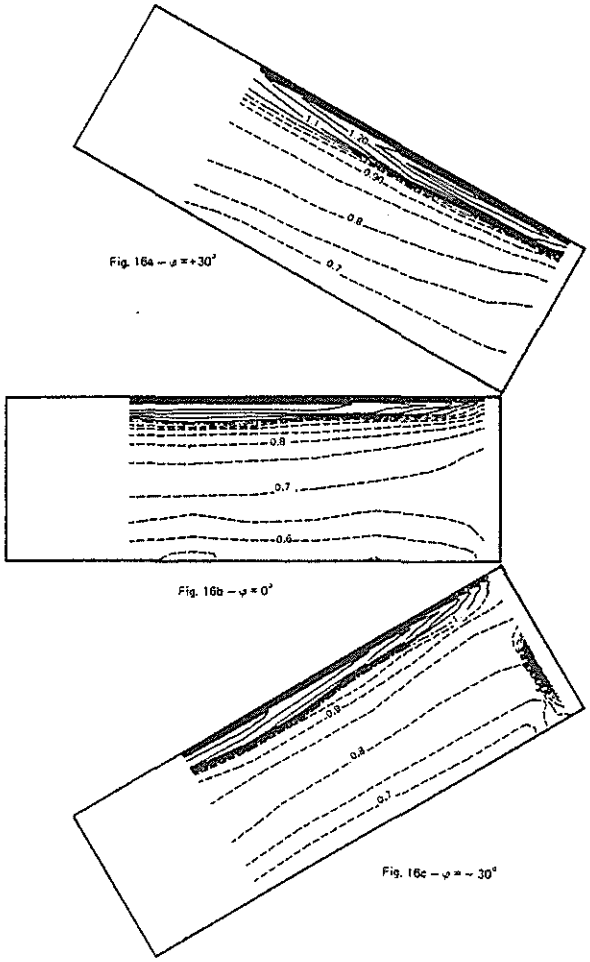

Fig. 16 – Iso-Mach lines on the upper surface . $M_N = 0.604$; $\alpha_N = 5.^\circ 6$.

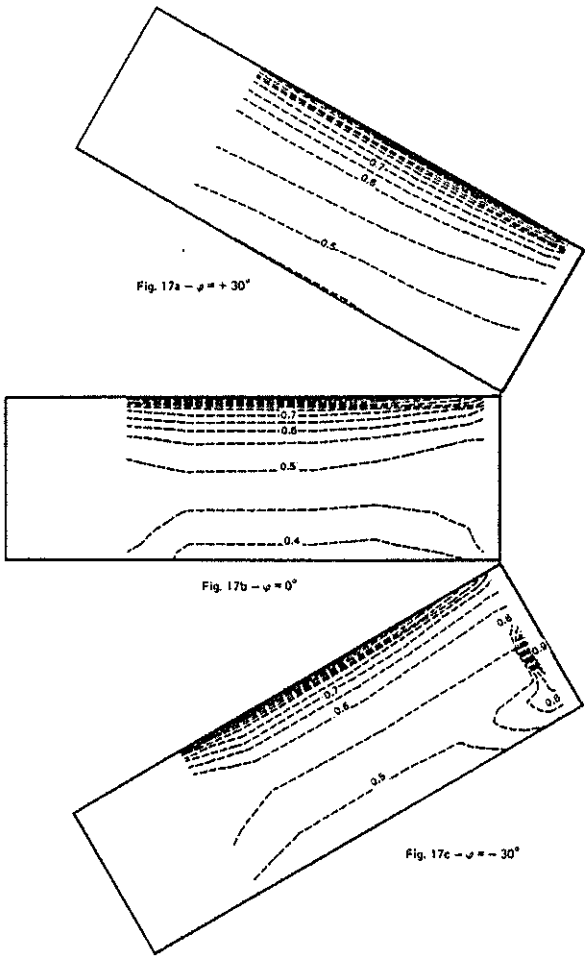

Fig. 17 – Iso-Mach lines on the upper surface.
$M_N = 0.402$; $\alpha_N = 11.^\circ 1$.

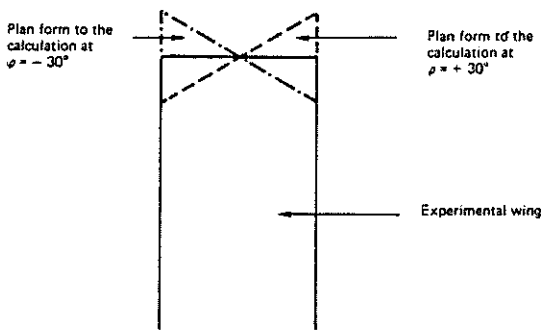

Fig. 18 – Calculated and experimental tip shapes.

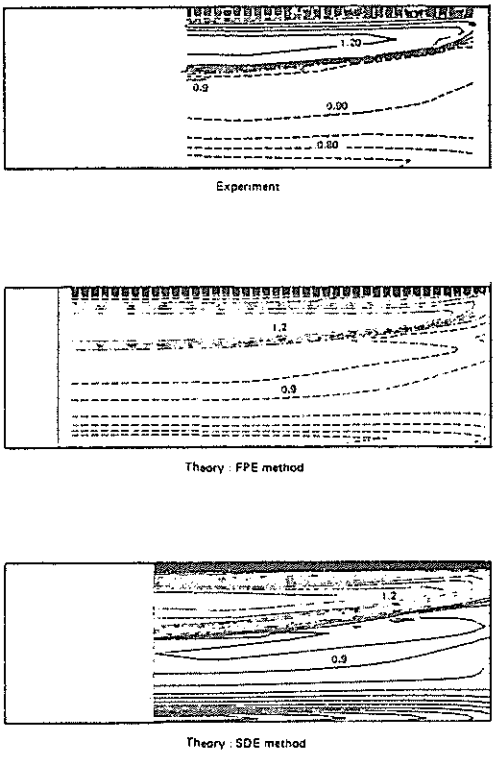

Fig. 19 — Theory-experiment comparison. Iso-Mach lines on the upper surface. Zero sweep $M_0 = 0.831$; $\alpha = -1.^\circ 5$.

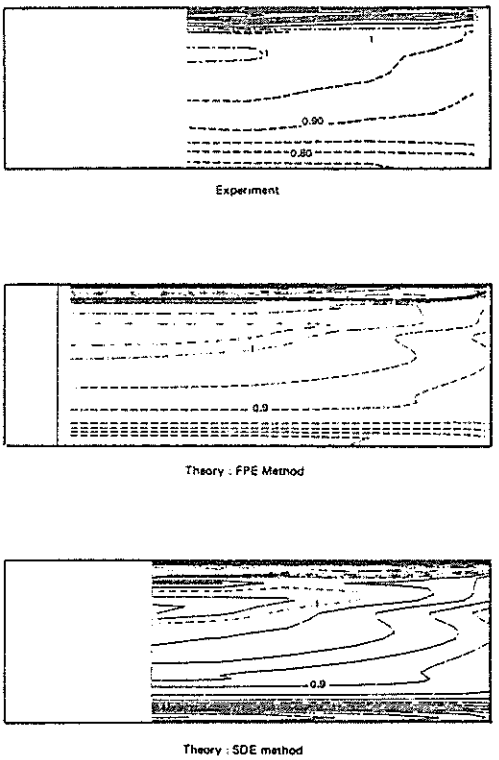

Fig. 20 — Theory-experiment comparison. Iso-Mach lines on the lower surface. Zero sweep $M_0 = 0.831$; $\alpha = -1.^\circ 5$.

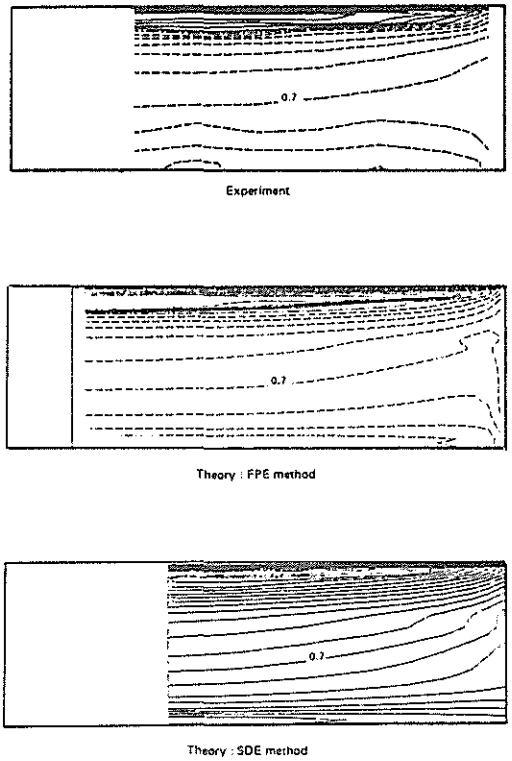

Fig. 21 — Theory-experiment comparison. Iso-Mach lines on the upper surface. Zero sweep $M_0 = 0.6$; $C_L \simeq 0.6$; $\alpha = 5.^\circ 6$.

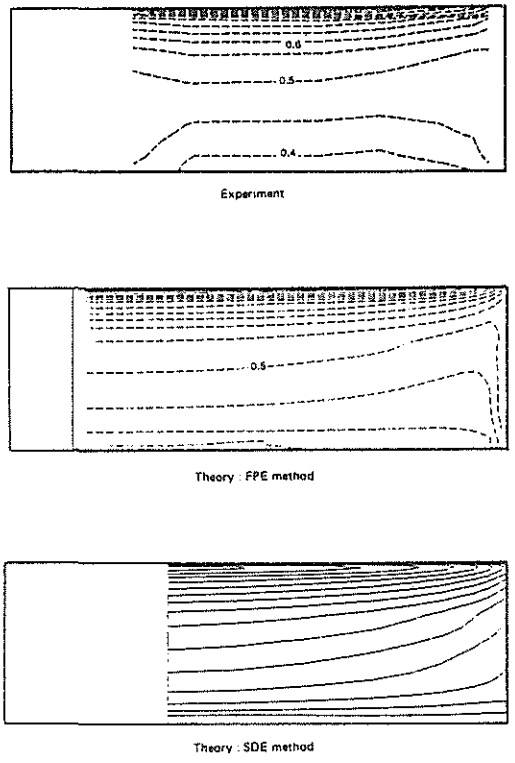

Fig. 22 — Theory-experiment comparison. Iso-Mach lines on the upper surface. Zero sweep $M_0 = 0.4$; $\alpha = 11^\circ$.

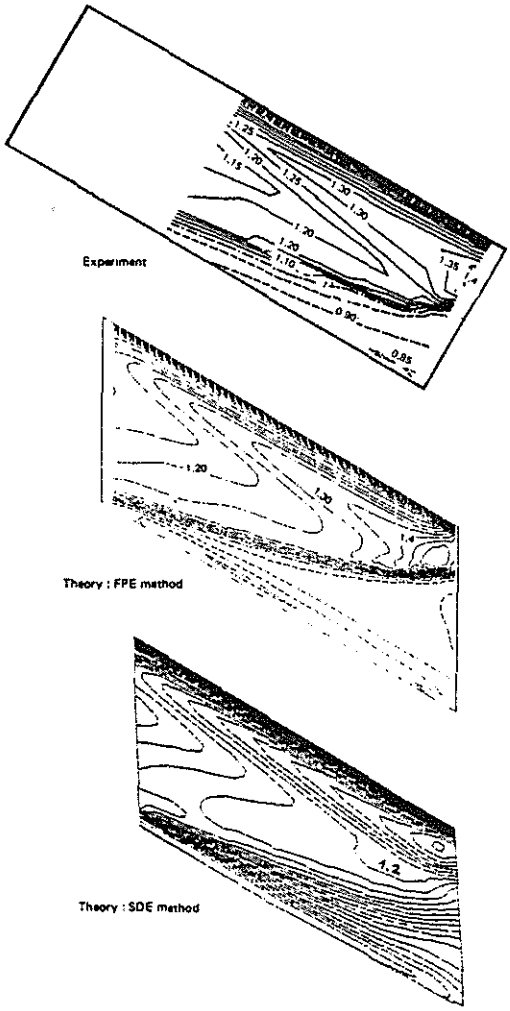

Fig. 23 – Theory-experiment comparison. Iso-Mach lines on the upper surface. Positive sweep + 30°. $M_N = 0.835$; $\alpha_N = -1.°5$.

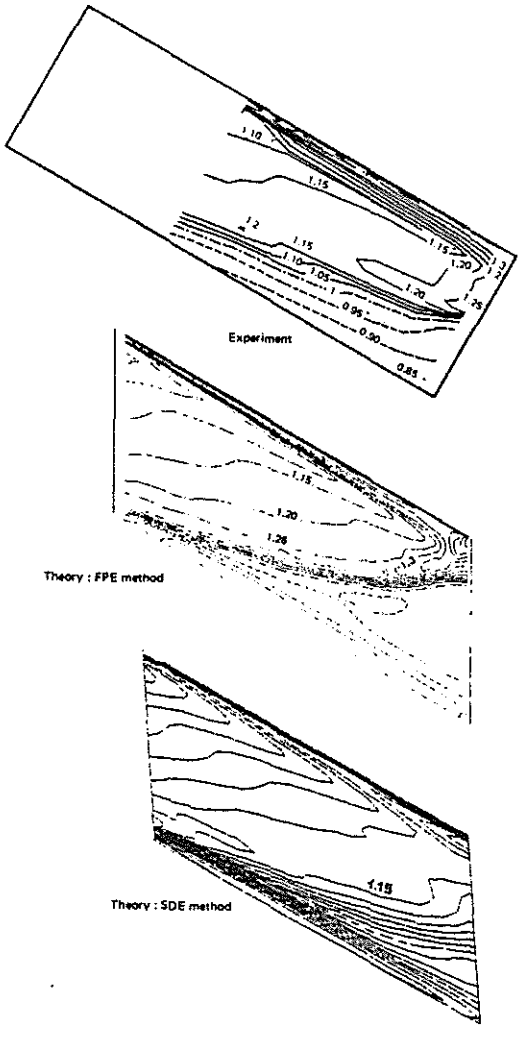

Fig. 24 – Theory-experiment comparison. Iso-Mach lines on the lower surface. Positive sweep + 30°. $M_N = 0.835$; $\alpha_N = -1.°5$.

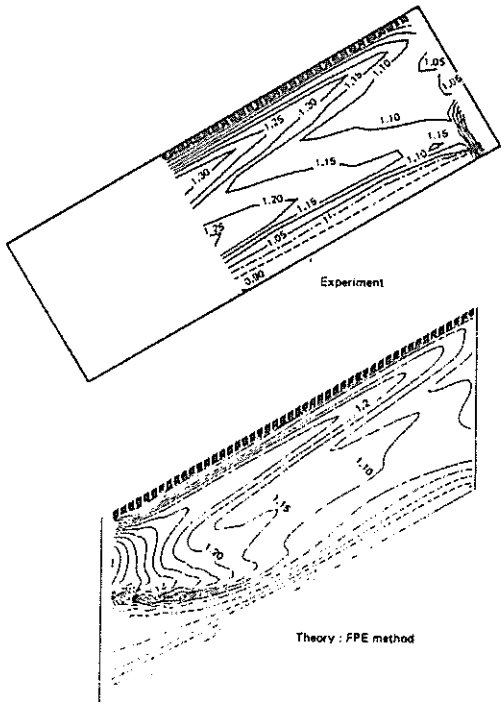

Fig. 25 — Theory-experiment comparison. Iso-Mach lines on the upper surface. Negative sweep — 30°. M_N = 0.831 ; $\alpha_N = -1.5$.

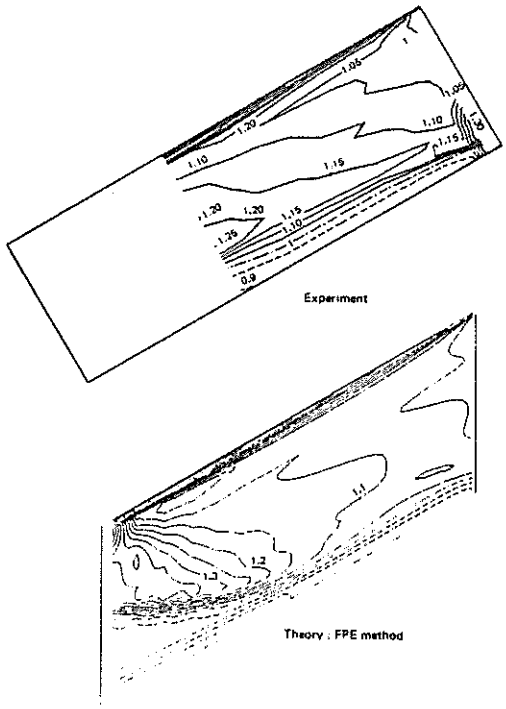

Fig. 26 — Theory-experiment comparison. Iso-Mach lines on the lower surface. Negative sweep — 30°. M_N = 0.831 ; $\alpha_N = -1.5$.

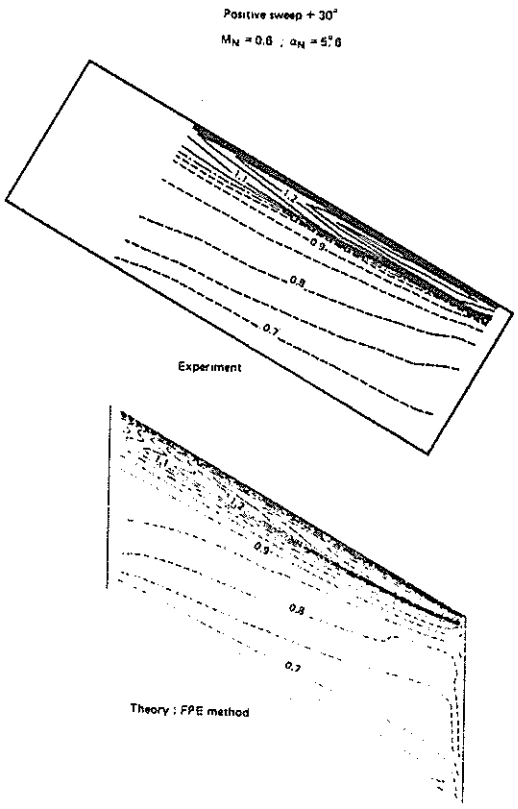

Fig. 27 — Theory-experiment comparison. Iso-Mach lines on the upper surface. Positive sweep + 30°. M_N = 0.6 ; $\alpha_N = -1.5$.

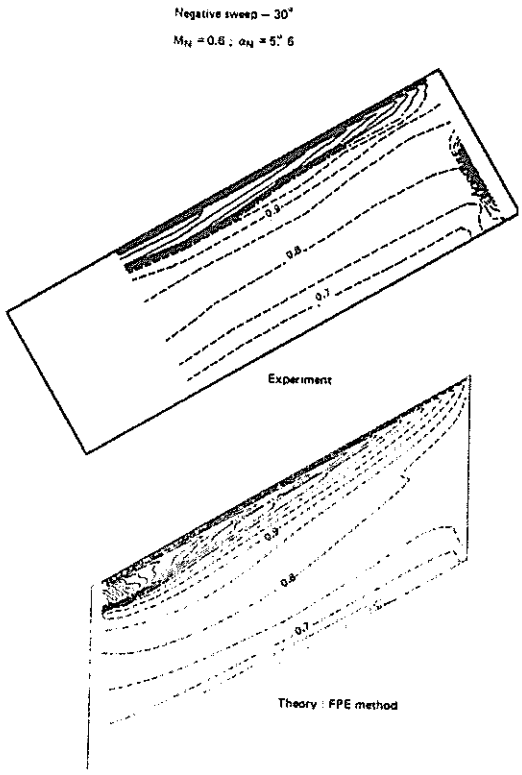

Fig. 28 — Theory-experiment comparison. Iso-Mach lines on the upper surface. Negative sweep — 30°. M_N = 0.6 ; $\alpha_N = -1.5$.

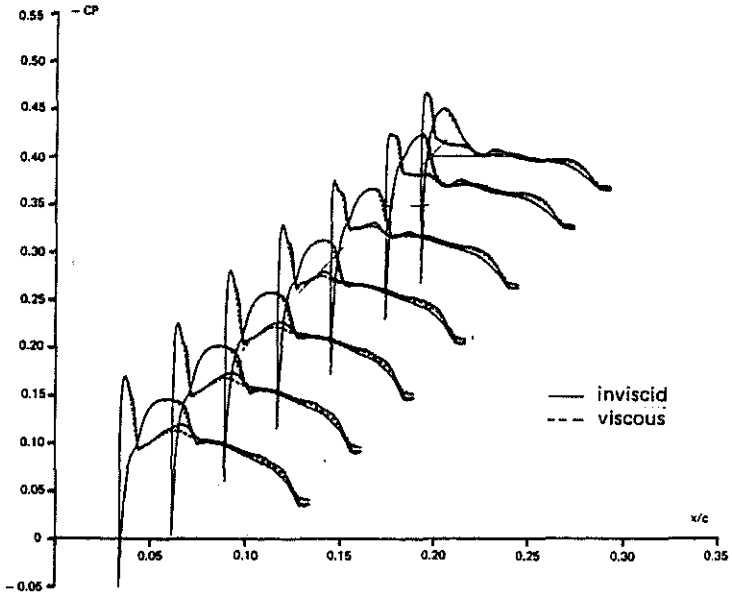

Fig. 29 – Viscosity effects at zero sweep. $M_0 = 0.831$, $C_z \cong 0$, $\alpha = -1.^\circ 5$.

Fig. 30 – Viscosity effects at positive sweep + 30° . $M_N = 0.831$, $C_z \cong 0$, $\alpha_N = -1.^\circ 5$.

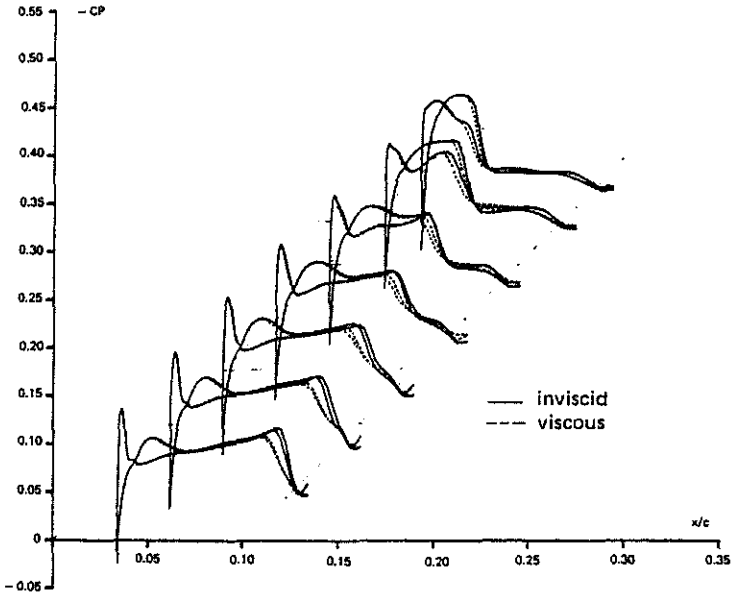

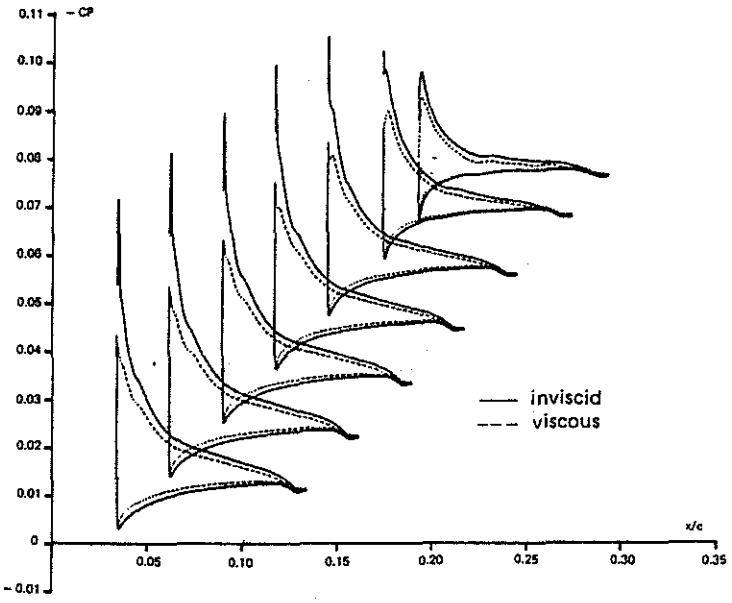

Fig. 31 – Viscosity effects at zero sweep −30°. $M_0 = 0.402$, $\alpha = 11.^\circ 1$.